ELSEVIER

Surface Science 342 (1995) L1131–L1136

surface science

Surface Science Letters

Stability of disk and stripe patterns of nanostructures at surfaces

P. Zeppenfeld, M.A. Krzyzowski, Ch. Romainczyk, R. David, G. Comsa

Institut für Grenzflächenforschung und Vakuumphysik, Forschungszentrum Jülich, D-52425 Jülich, Germany

H. Röder, K. Bromann, H. Brune, K. Kern

Institut de Physique Expérimentale, EPF Lausanne, PHB-Ecublens, CH-1015 Lausanne, Switzerland

Received 26 June 1995; accepted for publication 21 August 1995

Abstract

The ordering of two-dimensional Ag islands embedded in the Pt(111) surface layer has been investigated using He-atom scattering and scanning tunneling microscopy. At lower Ag coverage the embedded islands consist of compact clusters (disks) arranged into a short-range ordered two-dimensional array. At higher coverage the Ag islands have an elongated shape leading to a "labyrinthine" pattern of regularly spaced meandering stripes. As the temperature is increased, both the disk and stripe arrays of embedded Ag clusters transform reversibly into a disordered 2D Ag–Pt mixture. The observed behavior is explained in terms of strain-induced long-range interactions.

Keywords: Atom–solid scattering and diffraction – elastic; Low index single crystal surfaces; Platinum; Scanning tunneling microscopy; Silver; Surface stress; Surface structure, morphology, roughness, and topography

Competing interactions give rise to a variety of complex structures at surfaces. In particular, the interplay between short-range attractive and long-range repulsive forces can lead to the formation of domain patterns of equally sized domains (islands), arranged into a regular, periodic pattern [1–8]. Such complex domain structures have been observed in different environments such as amphilic monolayers at the air–water interface [1–3], thin ferrimagnetic garnet films [4], and strained adlayers at crystal surfaces [5]. These systems are governed by long-range interactions of different physical origin: electrostatic or magnetic dipole forces and elastic interactions. For surface systems interacting via dipole interactions, the stability and phase diagram of the resulting domain structures has been investigated by theory [6–8] and computer simulation [9]. One of the intriguing results of these studies is that the phase diagram can comprise two basic domain morphologies: a two-dimensional array of compact domains (e.g. disks or squares) and a quasi one-dimensional arrangement of striped domains. The existence of disk and stripe phases and the transition between these phases has also been observed experimentally, e.g. in Langmuir monolayers [1–3].

Recently, it was proposed [10] that the formation of complex domain patterns observed on strained crystal surfaces governed by elastic forces [5,11,12] could likewise be described in terms of long-range repulsive interactions. In fact, the theoretical description of the dipolar and elastic interactions turns out to be virtually identical [11]. This is due to the fact

SSDI 0039-6028(95)00891-8

that in both cases the "effective" repulsion between domain boundaries scales as $1/r^2$, where r is the separation between these boundaries.

As a consequence of this formal analogy, it is interesting to explore whether both stable disk and striped domain morphologies can actually be observed in strained surface systems in a similar way as in dipolar systems. In fact, a transition from a compact to elongated island shape was recently observed for strained Ag islands grown on Si(001) [13]. Although no particular arrangement of the Ag islands was reported, the shape of a *single* island can by itself be regarded as a manifestation of the role of effective long-range interactions: the competition between the creation of domain boundaries (island edges) and the long-range interaction between them determine the island shape.

Here we report the first observation of stable disk and striped domain shapes and patterns for a strained surface system, namely Ag embedded in the topmost layer of Pt(111). The embedded Ag nanostructures are prepared either by growing submonolayers of Ag at 300 K on Pt(111) followed by annealing at 700 K or by directly depositing Ag at 700 K. Both procedures lead to the formation of a two-dimensional "mixture" consisting of Ag clusters dissolved in the topmost Pt layer ($\Theta_{Ag} < 0.5$ ML) and Pt clusters inside a Ag matrix layer (0.5 ML $< \Theta_{Ag} < 1$ ML), respectively [14]. Once formed at elevated temperatures, this surface-confined mixture is stable upon recooling to room temperature. The stability of the embedded clusters was attributed to the balance of the strain relaxation (due to of the 4% lattice misfit between Ag and Pt) and the line tension associated with the total Ag–Pt boundary length [10,16].

The shape of the embedded Ag nanostructures and their relative arrangement have been studied by scanning tunneling microscopy (STM) and thermal energy atom scattering (TEAS) as a function of coverage and temperature. The two types of experiments were performed in separate ultrahigh vacuum (UHV) systems and on different samples. In both cases the sample was processed in the same way: The Pt(111) surface was cleaned and characterized in situ and a submonolayer amount of Ag was evaporated onto the Pt(111) surface by means of a Knudsen cell. Depending on the preparation procedure (see above) the sample was kept at 700 K during or heated to 700 K after Ag deposition in order to form the surface-confined Ag–Pt mixture.

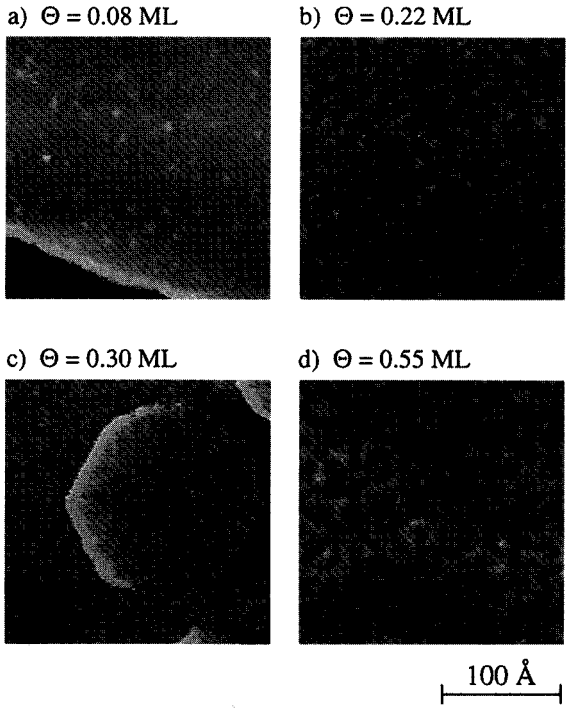

Fig. 1. Constant-current STM topographs (225 Å×225 Å) of a Pt(111) surface after deposition of submonolayer amounts of Ag annealed at elevated temperatures ($T > 700$ K), and imaged at 400 K: (a) Ag-coverage: $\Theta_{Ag} = 0.08$ ML, annealing temperature: $T =$ 700 K; (b) $\Theta_{Ag} = 0.22$ ML, $T = 850$ K; (c) $\Theta_{Ag} = 0.30$ ML, $T = 800$ K; (d) $\Theta_{Ag} = 0.55$ ML, $T = 850$ K. Note that in taking (b) and (c) a high-pass filter was used which enhances the contrast for steep changes of the tip-height. (a) and (d) are regular grey-scale images of the tip-height.

The STM topographs presented in Fig. 1 clearly show the different morphology of the Ag–Pt surface layer as a function of the Ag coverage. The images have been recorded at 400 K after annealing to $T > 700$ K. At low coverage (Figs. 1a and 1b, $\Theta_{Ag} <$ 0.25 ML) the embedded Ag atoms aggregate into small disk-shaped islands, about 10 Å in diameter, which appear as bright dots (~ 0.6 Å high) within the darker Pt surface. At higher Ag coverage (Figs. 1c and 1d, $\Theta_{Ag} > 0.3$ ML) the islands have an elongated shape and are arranged into a striped "labyrinthine" pattern. Obviously, the relative arrangement of the Ag disks or stripes is far from being perfectly hexagonal or one-dimensionally

striped. Nevertheless, there exists a certain degree of local order in that neighboring islands are separated preferentially by a distance of roughly 30 Å. This residual order of the island arrangement becomes more evident in the He diffraction spectra shown in Fig. 2c. For the stripe as well as for the disk configuration (not shown here) the diffraction profiles exhibit broad diffraction features at a parallel wave vector transfer $|Q| \approx 0.2$ Å^{-1}. These features are most pronounced for low surface temperature and indicate a lateral periodicity on the surface of $D = 2\pi/|Q| \approx 30$ Å. This value is in good agreement with the average distance between embedded Ag islands extracted from the STM images.

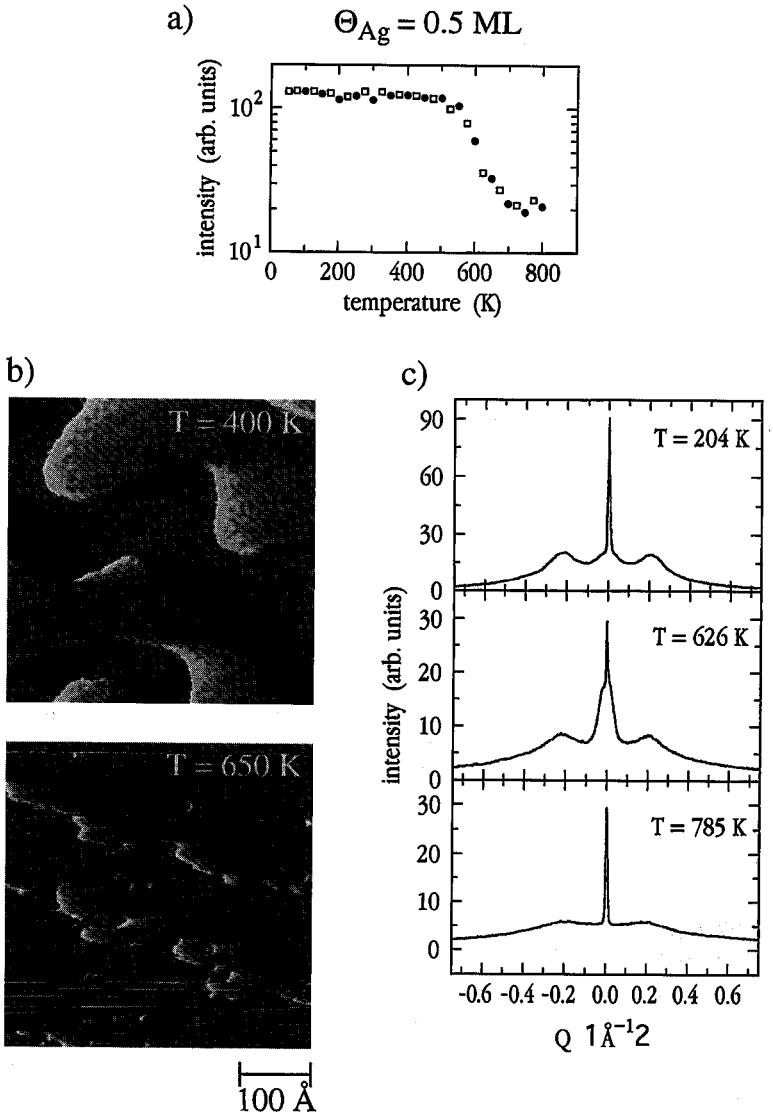

Fig. 2. Intensity (peak height) of the specularly reflected He-beam (a), He diffraction spectra (c) and STM topographs (450 Å × 450 Å) of the Ag–Pt(111) mixture for $\Theta_{Ag} = 0.5$ ML (striped phase) taken at different temperatures (b). Open and filled symbols in (a) correspond to measurements taken during increasing and decreasing the surface temperature, respectively. The He-diffraction profiles in (c) were recorded along the [11$\bar{2}$]-direction using a He-beam energy of 21.6 meV and fixed total scattering angle ($\vartheta_i + \vartheta_f = 90°$).

The STM topographs in Fig. 1 are remarkably similar to the patterns obtained in a recent computer simulation of a dipolar lattice gas for similar coverages [9]. They should also be compared to the disk and stripe arrangements observed in Langmuir monolayers [1–3], in which, however, the structures occur on a much larger, mesoscopic length scale.

In the following we will demonstrate that the transition from a disk to a stripe pattern with increasing coverage can be explained in a simple, straightforward way. We have shown in a recent letter [10] that the formation and the variation of the strain-induced pattern can be described within a simple analytical model based on the energy balance between the free energy γ associated with the creation and elastic relaxation of a domain boundary and the long-range effective repulsion $\propto \sigma/r^2$ between these boundaries. We emphasize that this model does not explicitly include effects due to the presence of corners or kinks along the boundary, nor does it account for the thermal disordering of the domain pattern. Therefore, the model can only provide a qualitative description of the general behavior. The excess free energy per unit area gained by formation of a perfectly regular domain pattern can be expressed as [10,17]:

$$\Delta F = \alpha\frac{\gamma\Theta}{D} + \frac{\alpha}{2}\frac{\sigma\Theta}{D}\left(\frac{1}{(D-l)^2} + \frac{1}{l^2}\right), \qquad (1)$$

where l and D characterize the domain width and separation, respectively, and α denotes the number of nearest-neighbor domains. For a stripe pattern $\alpha = 2$, for a checkerboard array $\alpha = 4$, and for a hexagonal arrangement of hexagon-shaped disks $\alpha = 6$. The main difference between the 2D arrangement of disk-like domains (squares or hexagons) and the 1D arrangement of stripe domains, is the variation of l and D with coverage Θ: For the minimum energy configurations the domain size $l(\Theta)$ and the periodicity $D(\Theta)$ for the stripe pattern are given by:

$$l(\Theta) = c_1\sqrt{1 + \frac{\Theta^2}{(1-\Theta)^2}},$$

$$D(\Theta) = c_1\sqrt{\frac{1}{\Theta^2} + \frac{1}{(1-\Theta)^2}}, \qquad (2)$$

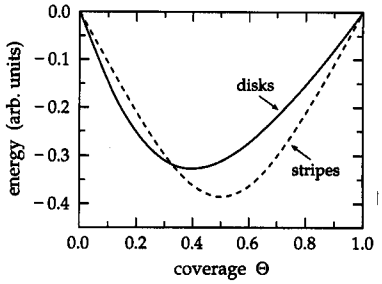

Fig. 3. Excess free energy as a function of coverage after formation of regularly ordered domain patterns of 2D and 1D symmetry, corresponding to a disk-phase (solid line) and stripe-phase (dashed line), respectively. The excess free energy for each coverage is calculated according to (1) for the minimum energy configurations of a perfectly ordered disk- and stripe-phase as given by (2) and (3). The parameters are $c_1 = 1.22$ ($\sigma_1 = 1$, $\gamma_1 = -1$) for the stripe-phase and $c_2 = 1.64$ ($\sigma_2 = 1$, $\gamma_2 = -1.8$) for the disk-phase which was modelled as a checkerboard array of square domains ($\alpha = 4$).

while for the disk pattern the result becomes:

$$l(\Theta) = c_2\sqrt{1 + \frac{\Theta}{(1-\sqrt{\Theta})^2}},$$

$$D(\Theta) = c_2\sqrt{\frac{1}{\Theta} + \frac{1}{(1-\sqrt{\Theta})^2}}. \qquad (3)$$

The proportionality constants $c_1 = \sqrt{-3\sigma_1/2\gamma_1}$ and $c_2 = \sqrt{-3\sigma_2/2\gamma_2}$ are given by the ratio between the relaxation energy and the strength of the repulsive interaction per unit length of a boundary. The indices 1 and 2 take into account that these values will, in general, be different for the stripe and disk configurations, e.g. due to the surface anisotropy. In Fig. 3 we have plotted the excess free energy ΔF obtained after substituting the minimum energy configurations (2) and (3) into (1). The relative position of the two curves determines whether the disk or stripe phase will be energetically preferred. Three different scenarios are possible: if $c_1 \ll c_2$ the stripe pattern will be stable for all coverages. If $c_1 \gg c_2$ only the disk pattern will be observed. In the intermediate regime, where $c_1 \approx c_2$ the two curves can cross such that for low coverage the disk pattern is energetically stable while at higher coverage the stripe pattern is preferred. In this case the model would predict a transition from the disk to the stripe

phase via an intermediate coexistence region whose composition is given by the "lever rule" for binary systems [18]. Note that the present model does not include the possibility for a continuous transition from a compact to an elongated shape of an individual island. This is, however, what appears to occur in the real physical system (see e.g. Fig. 1c). We, therefore, believe that the model does not correctly describe the Ag/Pt(111) patterns in the 2D–1D transition regime. We emphasize that due to the particular shape of the two curves in Fig. 3 the present model predicts that the opposite sequence, namely a transition from a stripe to a disk phase with increasing coverage cannot occur for coverages $\Theta <$ 0.5 ML. Note, however, that symmetrically above 0.5 ML a similar transition from the striped phase to a hole ('anti-disk') phase is expected. Since the different shape of the two curves in Fig. 3 is due to the different scaling of l and D with the coverage Θ for the 1D stripe and 2D disk patterns (eqs. (2) and (3), respectively) the disk to stripe transition in this simple model can be understood on purely geometric grounds.

Until now we have demonstrated the *existence* of disk and stripe domain shapes and patterns in the Ag–Pt(111) system without considering the *stability* of these patterns. To learn whether the observed structures are true equilibrium patterns (as expected from theory and simulation [6–12]) or merely the result of surface kinetics, we have studied the thermal stability of the embedded Ag island structure. The experimental results are summarized in Fig. 2 for the striped morphology.

The intensity of the specularly reflected He-beam ($Q = 0$) as a function of the temperature is shown in the top panel of Fig. 2. This provides a measure of the scattering factor of the *individual* islands and is, therefore, sensitive to changes of the island shape as well as to the number of surface defects [19]. The sharp intensity drop at a surface temperature $T \sim 550$ K marks the beginning of the disordering of the striped domain pattern. The onset of the deterioration of the domain structure is also revealed in the He diffraction spectra shown in Fig. 2c: For $T > 550$ K the intensity of the diffraction signatures at $|Q| \approx 0.2$ Å^{-1} continuously decreases with respect to the specular intensity and vanishes almost completely at around 700 K [20].

A possible and likely scenario for the thermal disordering of the domain structure is the increased meandering of the stripes followed by the dissolution of the stripes into smaller structures. Both disordering mechanisms would be accompanied by a proliferation of the total length of the Ag–Pt domain boundaries, which would account for the observed strong decrease of the specular intensity above 550 K.

In addition to the specular intensity decrease and the disappearance of the diffraction satellites at $|Q| \approx 0.2$ Å^{-1}, another interesting feature is observed in the diffraction spectra during the disordering of the striped phase: In the transition region between 550 K and 700 K, a triangular-shaped foot develops underneath the specular peak, centered around $Q = 0$ (see, for instance, the spectrum for $T = 626$ K in Fig. 2b). We note that a very similar diffraction feature was observed in He-scattering from a Ni(110) surface covered with a monolayer of hydrogen [21]. The triangular peak was then attributed to atomic size defects, namely missing hydrogen atoms in an otherwise perfectly ordered adlayer. In the present case the same distinctive feature could arise from small Ag or Pt defects which are formed during the disordering of the striped phase.

This interpretation is supported by the STM studies. In Fig. 2b we present two STM topographs characterizing the morphology of the Ag–Pt(111) surface mixture for $\Theta_{Ag} = 0.5$ ML at temperatures of 400 K and 650 K, respectively. At the higher temperature the labyrinthine pattern has completely disappeared in the STM topograph; the terraces are imaged completely flat, and no contrast arising from the different Ag and Pt imaging heights is seen [22]. We interpret this as evidence for a completely disordered 2D Ag–Pt phase at elevated temperatures. In such a phase Ag and Pt atoms are mixed randomly in a dense packing, and the surface appears flat in the STM. More information on the atomic structure of the disordered 2D mixed phase could be obtained from atomic resolution images, which we were not, however, able to obtain from this system at elevated temperatures. The thermal dissolution of the Ag cluster is preceded by a gradual disordering of the domain pattern. At temperatures around 600 K the meandering stripes of embedded Ag clusters are still visible in the STM images (not shown here) but are

characterized by an increased interfacial width and large local fluctuations.

Both, STM observations and He-scattering measurements thus support a thermal disordering scenario in which the Ag stripes would disorder by forming small protrusions followed eventually by the dissolution into small Ag clusters or individual Ag atoms. This picture is also in agreement with the results obtained in the computer simulation of the thermal disordering of the striped phase in Ref. [9]. We would, therefore, expect the Ag–Pt striped phase to look similar to the "snapshots" of the Monte Carlo simulation shown in Fig. 3 of Ref. [9].

Finally, we emphasize that the disk phase undergoes a thermal disordering transition, too. In both cases the variation of the He-specular intensity with temperature as well as the corresponding changes in shape of the He-diffraction spectra are completely reversible. This strongly suggests that both the disk and stripe phase are, indeed, equilibrium structures stable at lower and higher coverage, respectively, and for surface temperatures below 700 K.

Acknowledgements

We acknowledge fruitful discussions with Max G. Lagally, Bene Poelsema, Rolf Schuster, Ian Robinson, and Georg Rosenfeld.

References

[1] M. Seul and M.J. Sammon, Phys. Rev. Lett. 64 (1990) 1903.
[2] K. To, S. Akamatsu, and F. Rondelez, Europhys. Lett. 21 (1993) 343.
[3] M. Seul and V.S. Chen, Phys. Rev. Lett. 70 (1993) 1658.
[4] M. Seul, L.R. Monar, L. O'Gorman, and R. Wolfe, Science 254 (1991) 1616.
[5] K. Kern, H. Niehus, A. Schatz, P. Zeppenfeld, J. Goerge, and G. Comsa, Phys. Rev. Lett. 67 (1991) 885.
[6] T. Garel and S. Doniach, Phys. Rev. B 26 (1982) 325.
[7] D. Andelman, F. Brochard, and J.-F. Joanny, J. Chem. Phys. 86 (1987) 3673.
[8] Y. Yafet and E.M. Gyorgy, Phys. Rev. B 38 (1988) 9145.
[9] M.M. Hurley and S.J. Singer, Phys. Rev. B 46 (1992) 5783.
[10] P. Zeppenfeld, M. Krzyzowski, Ch. Romainczyk, G. Comsa, and M.G. Lagally, Phys. Rev. Lett. 72 (1994) 2737.
[11] D. Vanderbilt, Surf. Sci. 268 (1992) L300; K.-O. Ng and D. Vanderbilt, Phys. Rev. B 52 (1995) 2177.
[12] V.I. Marchenko, JETP Lett. 55 (1992) 73.
[13] J. Tersoff and R.M. Tromp, Phys. Rev. Lett. 70 (1993) 2782.
[14] H. Röder, R. Schuster, H. Brune, and K. Kern, Phys. Rev. Lett. 71 (1993) 2086. The presence of small clusters at elevated temperatures was recognized in an earlier He-scattering study by Becker et al. [15], but the underlying mixing transition was misinterpreted as a fragmentation of Ag islands into small clusters adsorbed on *top* of the Pt(111) surface.
[15] A.F. Becker, G. Rosenfeld, B. Poelsema, and G. Comsa, Phys. Rev. Lett. 70 (1993) 477.
[16] J. Tersoff, Phys. Rev. Lett. 74 (1995) 434.
[17] H. Hörnis, J.R. West, E.H. Conrad, and R. Ellialtioglu, Phys. Rev. B47 (1993) 13055(RC).
[18] See e.g. R.A. Swalin, Thermodynamics of Solids (Wiley, New York, 1962) chapter 11.
[19] B. Poelsema and G. Comsa, Scattering of Thermal Energy Atoms, Springer Tracts in Modern Physics, Vol. 115 (Springer, Berlin, 1989).
[20] The specular intensity curves discussed here should not be confused with the specular reflectivity measurements by Becker et al. in Ref. [15]. The TEAS measurements of Becker et al. characterize the *irreversible* embedding transition of the adsorbed Ag islands into the topmost Pt layer while the specular intensity curves reported here characterize the *thermal equilibrium behavior* of the already embedded Ag nanostructures.
[21] W.A. Schlup and K.H. Rieder, Phys. Rev. Lett. 56 (1986) 73.
[22] The appearance of flat terraces in the STM is not related to the enhanced mobility of atoms and cluster at high temperatures. In the 650 K image in Fig. 2b) steps and defects (small holes in the Ag–Pt layer) are found to be "stable" on the time scale necessary to record an image.